

## On the Distance of SGR 1935+2154 Associated with FRB 200428

SHU-QING ZHONG,<sup>1,2</sup> ZI-GAO DAI,<sup>1,2</sup> HAI-MING ZHANG,<sup>1,2</sup> AND CAN-MIN DENG<sup>3,4</sup>

<sup>1</sup>*School of Astronomy and Space Science, Nanjing University, Nanjing 210093, China; dzg@nju.edu.cn*

<sup>2</sup>*Key laboratory of Modern Astronomy and Astrophysics (Nanjing University), Ministry of Education, Nanjing 210093, China*

<sup>3</sup>*Department of Astronomy, School of Physical Sciences, University of Science and Technology of China, Hefei, Anhui 230026, China*

<sup>4</sup>*CAS Key Laboratory for Research in Galaxies and Cosmology, Department of Astronomy, University of Science and Technology of China, Hefei 230026, Anhui, China*

*Submitted to The Astrophysical Journal Letters on 2020 May 22*

### ABSTRACT

Owing to the detection of a fast radio burst (FRB) 200428 from soft gamma-ray repeater (SGR) 1935+2154 associated with a hard X-ray counterpart, the distance of SGR 1935+2154 potentially hosted in the supernova remnant (SNR) G57.2+0.8 can be revisited. Under the assumption that the SGR and the SNR are realistically related, in this Letter, by investigating the dispersion measure (DM) of the FRB contributed by the foreground medium of our Galaxy and the local environments and combining with the observational constraints, we find that the distance is in a narrow range of 9.06 – 9.11 kpc and the SNR radius falls into 14.5 – 14.6 pc since the local DM contribution is as low as 0 – 5 pc cm<sup>-3</sup>. These results are basically consistent with the previous studies but appear to be tighter. Additionally, the estimate for the Faraday rotation measure of the SGR and SNR is also available.

*Keywords:* Magnetars (992); Soft gamma-ray repeaters (1471); Radio transient sources (2008)

### 1. INTRODUCTION

Very recently, an extremely bright millisecond-timescale radio burst from the Galactic magnetar SGR 1935+2154 was reported by The CHIME/FRB Collaboration et al. (2020) and Bochenek et al. (2020). More excitingly, its associated X-ray counterpart was also detected by Insight-HXMT (Zhang et al. 2020b,c,d; Li et al. 2020), AGILE (Tavani et al. 2020), INTEGRAL (Mereghetti et al. 2020), and Konus-Wind (Ridnaia et al. 2020) telescopes. In addition, a subsequent highly polarised transient pulsating radio burst was detected by the FAST radio telescope with Faraday rotation measure (RM) +112.3 rad m<sup>-2</sup> (Zhang et al. 2020a), approximately consistent with RM = +116 ± 2 ± 5 rad m<sup>-2</sup> of FRB 200428 (The CHIME/FRB Collaboration et al. 2020). Obtained from the previous investigations, we know that the magnetar SGR 1935+2154 has a spin period  $P \simeq 3.24$  s, a spin-down rate  $\dot{P} \simeq 1.43 \times 10^{-11}$  ss<sup>-1</sup>, a surface dipole magnetic field strength  $B_p \simeq 2.2 \times 10^{14}$  G, an age  $t \sim 3.6$  kyr, and a spin-down luminosity  $L_{sd} \sim 1.7 \times 10^{34}$  erg s<sup>-1</sup> (Israel et al. 2016), possibly hosted in the Galactic supernova remnant (SNR) G57.2+0.8 (Gaensler 2014).

In the literature, however, the distance of SNR G57.2+0.8 has a large range and remains highly de-

bated even though various methods have been used, e.g., the statistical radio surface-brightness-to-diameter relation ( $\sim 9.1$  kpc; Pavlović et al. 2013), the empirical relation between the hydrogen column density  $N_H$  and the dispersion measure (DM) (11.7 ± 2.8 kpc; Surnis et al. 2016), and the local standard of rest (LSR) velocity measure via HI absorption feature (12.5 ± 1.5 kpc; Kothes et al. 2018), (4.5–9.0 kpc; Ranasinghe et al. 2018), and via CO gas towards the SNR (6.6 ± 0.7 kpc; Zhou et al. 2020). For SGR 1935+2154, Kozlova et al. (2016) gave an upper limit < 10 kpc through the scattered link between the squares of the radii of the emitting areas and the corresponding black-body temperatures.

In this Letter, we assume that SGR 1935+2154 is indeed associated with SNR G57.2+0.8 and the SNR has the same age with SGR 1935+2154, then use the DM by combining with observational constraints to estimate the distance in Section 2. Our results are displayed in Section 3. A discussion on RM estimate and results is arranged in Section 4, and conclusions are drawn in Section 5.

### 2. DM ESTIMATE

From the observations of CHIME and STARES radio telescopes (The CHIME/FRB Collaboration et al. 2020; Bochenek et al. 2020), FRB 200428 has analogous

observed DM ( $DM_{\text{obs}} = 332.7206 \pm 0.0009 \text{ pc cm}^{-3}$  and  $332.702 \pm 0.008 \text{ pc cm}^{-3}$ ). The  $DM_{\text{obs}}$  is mainly contributed by the foreground interstellar medium (ISM) in our Galaxy ( $DM_{\text{Gal}}$ ), the magnetar wind nebula ( $DM_{\text{MWN}}$ ), and the SNR ( $DM_{\text{SNR}}$ ), that is,

$$DM_{\text{obs}} = DM_{\text{Gal}} + DM_{\text{MWN}} + DM_{\text{SNR}}, \quad (1)$$

where the foreground DM of our Galaxy is

$$DM_{\text{Gal}} = \int_0^D n_e(l) dl, \quad (2)$$

related to the distance  $D$  of SGR 1935+2154 via the Galactic electron density ( $n_e$ ) distribution NE2001 (Cordes & Lazio 2002) (or YMW16; Yao et al. 2017).

The  $DM_{\text{MWN}}$  is primarily attributed to O-mode wave and may be given by (e.g., Yu 2014; Cao et al. 2017; Yang & Zhang 2017)

$$DM_{\text{MWN}} \simeq 0.082 \text{ pc cm}^{-3} \mu_{\pm,4}^{2/3} B_{\text{p},14}^{4/3} P_0^{-11/3}, \quad (3)$$

where  $\mu_{\pm} = 10^4 \mu_{\pm,4}$  is the multiplicity parameter of the electron-positron pairs,  $B_p = 10^{14} B_{\text{p},14} \text{ G}$  is the dipole magnetic field, and  $P = 10^0 P_0 \text{ s}$  is the rotation period of the magnetar.

In regard to the  $DM_{\text{SNR}}$ , it depends on the ambient medium: constant density ISM or wind environment. So we consider the DM contribution by the SNR in two different scenarios as follows.

### 2.1. Constant ISM

It is widely accepted that an SNR has three phases after a supernova (SN) explosion in constant ISM scenario: (a) the free-expansion phase, (b) the Sedov-Taylor phase, (c) and the snowplow phase. Because SNR G57.2+0.8 has possibly reached the end of the Sedov-Taylor phase or entered the snowplow phase due to the non-detection of X-ray emission (Kothes et al. 2018; Zhou et al. 2020), the  $DM_{\text{SNR}}$  for the ionized medium (including shocked SN ejecta and shocked swept ambient medium<sup>1</sup>), can be estimated by

$$DM_{\text{SNR}} \simeq \begin{cases} 34 \text{ pc cm}^{-3} t_2^{2/5} E_{51}^{1/5} n_2^{4/5}, & t < t_{\text{SP}} \\ 81 \text{ pc cm}^{-3} t_3^{2/7} E_{51}^{0.225} n_2^{0.737}, & t > t_{\text{SP}} \end{cases} \quad (4)$$

during the Sedov-Taylor and snowplow phases (e.g., Yang & Zhang 2017; Piro & Gaensler 2018), where  $t =$

$10^i t_i \text{ yr}$ ,  $E = 10^{51} E_{51} \text{ erg}$  is the energy of the SN explosion, and  $n = 10^2 n_2 \text{ cm}^{-3}$  is the number density of a uniform ISM, as well as the snowplow time  $t_{\text{SP}} \simeq 3920 \text{ yr } E_{51}^{0.22} n_2^{-0.55}$  (e.g., Draine 2011). The corresponding SNR radius during different phases can be written by (e.g., Taylor 1950; Sedov 1959; Draine 2011; Yang & Zhang 2017)

$$R_{\text{SNR}} \simeq \begin{cases} 0.84 \text{ pc } t_2^{2/5} E_{51}^{1/5} n_2^{-1/5}, & t < t_{\text{SP}} \\ 2.44 \text{ pc } t_3^{2/7} E_{51}^{0.225} n_2^{-0.263}, & t > t_{\text{SP}} \end{cases} \quad (5)$$

Here we use the Sedov-Taylor radius independent of the mass of the SN ejecta as the SNR radius (Yang & Zhang 2017) rather than the blastwave radius depending on the mass of the SN ejecta (Piro & Gaensler 2018), which can be a good approximation when the SNR probably has reached the end of the Sedov-Taylor phase or entered the snowplow phase.

### 2.2. Wind Environment

In wind scenario, the SNR evolution has two phases: the early ejecta-dominated phase and the wind-dominated phase occurring at very late times, based on Piro & Gaensler (2018). During different phases, the  $DM_{\text{SNR}}$  is calculated by (see Table 2 of Piro & Gaensler 2018)

$$DM_{\text{SNR}} \simeq \begin{cases} 13 \text{ pc cm}^{-3} \mu_e^{-1} t_2^{-3/2} E_{51}^{-3/4} M_1^{5/4} K_{13}^{1/2}, & t < t_{\text{ch}} \\ 0.088 \text{ pc cm}^{-3} \mu_e^{-1} t_3^{-2/3} E_{51}^{-1/3} K_{13}^{4/3}, & t > t_{\text{ch}} \end{cases} \quad (6)$$

where  $\mu_e$  is the mean molecular weight per electron,  $M = M_1 \times 1 M_{\odot}$  is the mass of the SN ejecta,  $K = 5.1 \times 10^{13} \text{ g cm}^{-1} \dot{M}_{-5} v_6^{-1}$  (here, the mass-loss rate  $\dot{M}_{-5} = 10^{-5} M_{\odot} \text{ yr}^{-1}$  and the wind velocity  $v_6 = v_w / 10^6 \text{ cm s}^{-1}$ ), and the characteristic time  $t_{\text{ch}} = 1.9 \times 10^3 \text{ yr } E_{51}^{-1/2} M_1^{3/2} K_{13}^{-1}$  separating the two phases. This characteristic time corresponds to a radius  $R_{\text{ch}} = 16.8 \text{ pc } M_1 K_{13}^{-1}$ . Such that the SNR radius regarded as the blastwave radius can be related to  $R_{\text{ch}}$  and  $t_{\text{ch}}$  through the analytic functions (see Table 2 of Piro & Gaensler 2018)

$$R_{\text{SNR}} \simeq \begin{cases} 1.79 R_{\text{ch}} (t/t_{\text{ch}}) \left[ 1 + 0.33 (t/t_{\text{ch}})^{1/2} \right]^{-2}, & t < t_{\text{ch}} \\ [1.11 (t/t_{\text{ch}}) - 0.11]^{2/3} R_{\text{ch}}, & t > t_{\text{ch}} \end{cases} \quad (7)$$

## 3. DM RESULTS

<sup>1</sup> We assume the swept ambient medium is fully ionized in order to acquire an upper limit of the  $DM_{\text{SNR}}$ . However, we neglect the unshocked ambient medium in the upstream of the shock since it is neutral hydrogen dominated, as done in Piro & Gaensler (2018).

A very useful observational constraint for SNR G57.2+0.8 is that it is an almost circular source with an average diameter about  $10'$ , i.e., radius  $\theta_r \approx 5'.5$  (Kothes et al. 2018), which is relevant to the SNR radius via the distance of SGR 1935+2154

$$D = \frac{R_{\text{SNR}}}{\theta_r}. \quad (8)$$

Moreover, the observational constraints for  $\text{DM}_{\text{obs}}$ ,  $t$ ,  $B_p$ , and  $P$  are also known. Through the calculations of Equation (3), we find that the value of  $\text{DM}_{\text{MWN}}$  is far smaller than  $1 \text{ pc cm}^{-3}$  even if  $\mu_{\pm}$  is very large like  $10^6$ , so we safely ignore this term in Equation (1) for subsequent calculations.

In the ISM scenario for the SNR, utilizing Equations (1), (2)<sup>2</sup>, (4), (5), and (8), we can get a power-law relation with an index 1.0 between the explosion energy  $E$  and the ambient medium density  $n$ , as illustrated in the top panel of Figure 1. Moreover, it is obviously seen that the ambient medium density favors a relatively low value  $< 1 \text{ cm}^{-3}$ . Meanwhile, one can also acquire a narrow distance distribution  $D \simeq 9.06 - 9.11 \text{ kpc}$  (so a narrow SNR radius  $R_{\text{SNR}} \simeq 14.5 - 14.6 \text{ pc}$ ), and a limited  $\text{DM}_{\text{SNR}} \simeq 0 - 5 \text{ pc cm}^{-3}$  illustrating in the middle and bottom panels of Figure 1, within a typical explosion energy ranging from several  $10^{49} \text{ erg}$  to several  $10^{51} \text{ erg}$  (e.g., Pejcha & Prieto 2015; Lyman et al. 2016). Visibly, it can also be seen that the  $\text{DM}_{\text{SNR}}$  is very low at current age  $t = 3.6 \text{ kyr}$  of SGR 1935+2154, compared with the Galactic contribution  $\text{DM}_{\text{Gal}}$ .

For the wind environment towards the SNR, employing Equations (1), (2), (6)<sup>3</sup>, (7), and (8), we obtain a relation between the explosion energy  $E$  and the parameter  $K$  for  $M = 2 M_{\odot}$  (stripped-envelope SNe) and  $M = 10 M_{\odot}$  (red supergiant progenitors), as appeared in Figure 2. The parameter  $K$  declines sharply when the explosion energy  $E < 4 \times 10^{50} \text{ erg}$  ( $E < 2 \times 10^{51} \text{ erg}$ ) for  $M = 2 M_{\odot}$  ( $M = 10 M_{\odot}$ ), so we estimate the evolutions of other parameters by only considering the explosion energy  $E > 4 \times 10^{50} \text{ erg}$  ( $E > 2 \times 10^{51} \text{ erg}$ ) for  $M = 2 M_{\odot}$  ( $M = 10 M_{\odot}$ ). Other panels of Figure 2 exhibit that the distance spans  $D \simeq 9.06 - 9.11 \text{ kpc}$  and the DM contribution of the SNR occupies  $\text{DM}_{\text{SNR}} \simeq 0 - 5 \text{ pc cm}^{-3}$  for different ejecta mass. These results are in agreement with those in ISM scenario.

In summary, our results seem more compact even though they generally agree with those in previ-

ous studies by Pavlović et al. (2013), Surnis et al. (2016), Kothes et al. (2018), Ranasinghe et al. (2018), and Zhou et al. (2020) for SNR G57.2+0.8, and Kozlova et al. (2016) for SGR 1935+2154. The former methods in Pavlović et al. (2013), Surnis et al. (2016), and Kozlova et al. (2016) are empirical and statistical, with intrinsic large scatter. The latter methods seem to be more direct and their uncertainties mainly stem from the LSR velocity measure and the rotation curve of the Galaxy. In comparison, the distance estimate from DM in this paper is assumption-dependent and model-dependent but the results seem to be not significantly changeable in different models. The uncertainty in this method maybe primarily originate from the Galactic electron density distribution of YMW16 model.

#### 4. RM ESTIMATE

Similar to the DM estimate, the observed  $\text{RM}_{\text{obs}}$  should also has three parts: the foreground  $\text{RM}_{\text{Gal}}$  due to the Galactic ISM and permeating magnetic fields, the  $\text{RM}_{\text{MWN}}$  contributed by the magnetar wind nebula, and the  $\text{RM}_{\text{SNR}}$  resulted from the SNR, read as

$$\text{RM}_{\text{obs}} = \text{RM}_{\text{Gal}} + \text{RM}_{\text{MWN}} + \text{RM}_{\text{SNR}}. \quad (9)$$

(1) The first part  $\text{RM}_{\text{Gal}}$  can be expressed as

$$\text{RM}_{\text{Gal}} [\text{rad m}^{-2}] = 0.81 \int_0^D n_e [\text{cm}^{-3}] B_{\parallel} [\mu\text{G}] dl [\text{pc}] \quad (10)$$

where  $B_{\parallel}$  is the component of the Galactic magnetic field (GMF) parallel to the line of sight. RM is positive when the magnetic field points towards us. There is a general model of the GMF consisting of two different components: a disk field and a halo field (Prouza & Šmída 2003; Sun et al. 2008). The widely used disk field is the logarithmic spiral disk GMF model, which has two versions: the axisymmetric disk field (ASS model) and the bisymmetric disk field (BSS model) (e.g., Simard-Normandin & Kronberg 1980; Han & Qiao 1994; Stanev 1997; Tinyakov & Tkachev 2002). To estimate the  $\text{RM}_{\text{Gal}}$ , we consider the disk field with an ASS or BSS form and halo field with a basic form (Prouza & Šmída 2003; Sun et al. 2008; Jansson et al. 2009; Sun & Reich 2010; Pshirkov et al. 2011) as done in Lin & Dai (2016), combining with the Galactic free electron distribution  $n_e$  in Yao et al. (2017) and the distance  $D \simeq 9 \text{ kpc}$  from DM estimate. However, the  $\text{RM}_{\text{Gal}}$  has different values in different models or in same models but with different parameters, from several dozen to a few hundred  $\text{rad m}^{-2}$ , e.g.,  $\sim 670 \text{ rad m}^{-2}$  for ASS+halo and  $\sim 270 \text{ rad m}^{-2}$  for BSS+halo in Pshirkov et al. (2011), and  $-82 \text{ rad m}^{-2}$  for ASS+halo in Sun et al. (2008).

<sup>2</sup> Here, we adopt the YMW16 model whose code has been built-in the pyymw16 package of Python.

<sup>3</sup> We adopt  $\mu_e = 1$ . The values of  $\mu_e$  in a reasonable range cannot significantly influence the final results.

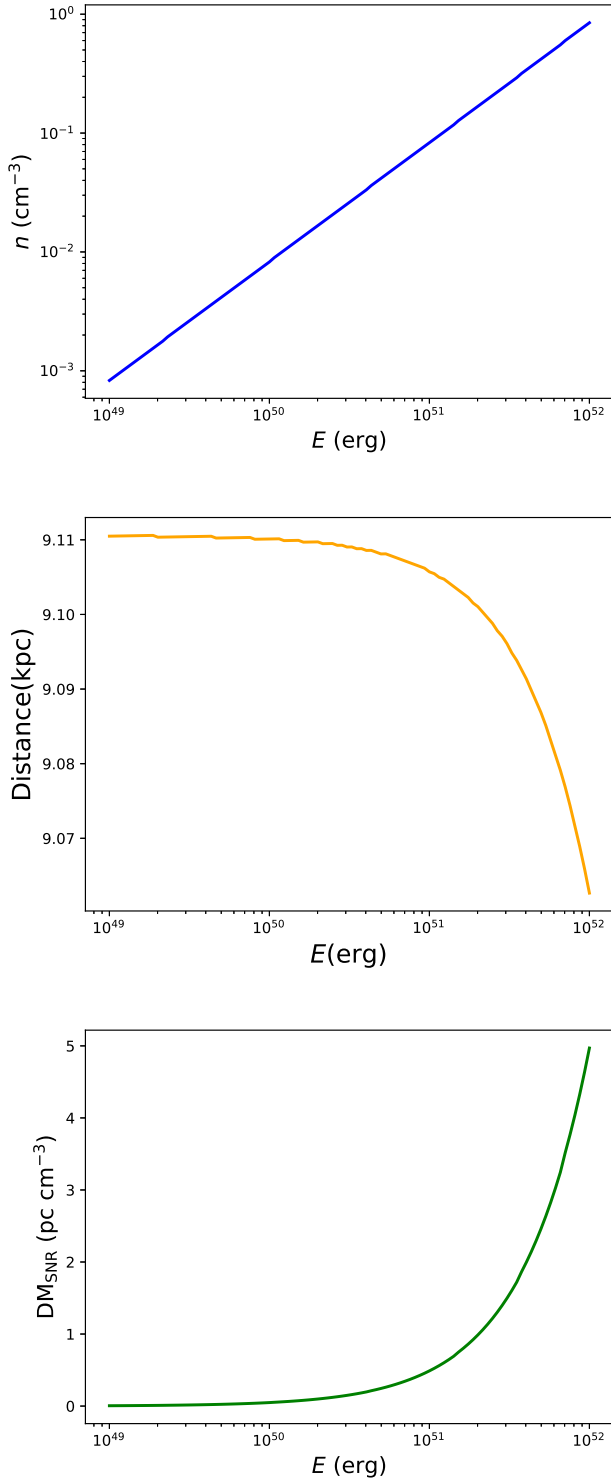


**Figure 1.** In the constant ISM for the SNR: (a) ambient medium density  $n$  as a power-law function of the energy of the SN explosion  $E$  (top panel); (b) the distance  $D$  of SGR 1935+2154 evolves with the explosion energy  $E$  (middle panel); (c) the  $DM_{\text{SNR}}$  contributed by the SNR is relevant to the explosion energy  $E$  (bottom panel).

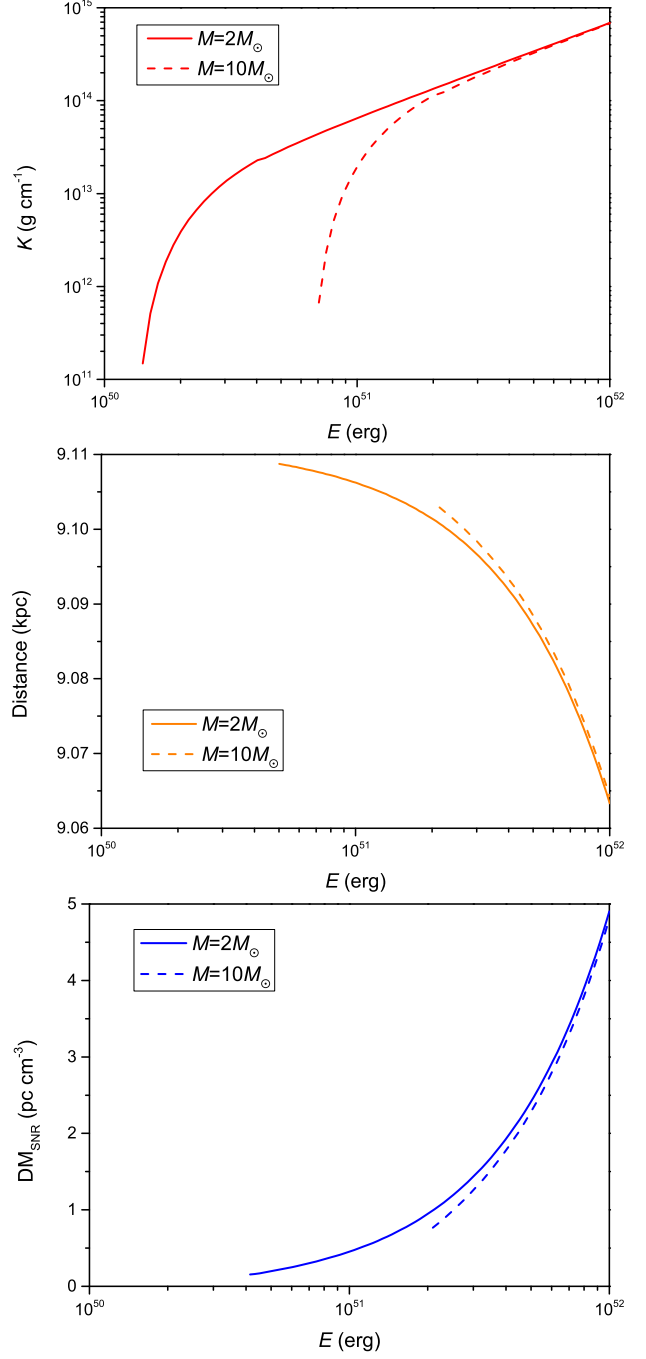


**Figure 2.** In the wind environment for the SNR: (a) the parameter  $K = 5.1 \times 10^{13} \text{ g cm}^{-1} \dot{M}_{-5} v_6^{-1}$  as a function of the energy  $E$  of the SN explosion (top panel); (b) same as the middle panel of Figure 1 (middle panel); (c) same as the bottom panel of Figure 1 (bottom panel).

Therefore, it cannot be well estimated by the GMF models. Nevertheless, [Kothes et al. \(2018\)](#) found that the foreground  $RM = +223 \pm 2 \text{ rad m}^{-2}$  for SNR G57.2+0.8 via the polarized intensity maps.

(2) The second part  $\text{RM}_{\text{MWN}}$  is primarily caused by the magnetar wind nebula due to the magnetar spin-down energy release. The magnetic field of the nebula at time  $t$  can be crudely estimated by (Metzger et al. 2017)

$$B_n \simeq \left( \frac{6\epsilon_B L_{\text{sd}} t}{R_n^3} \right)^{1/2}, \quad (11)$$

where  $\epsilon_B$  is the ratio of the magnetic energy to the shock energy. Assuming  $R_n \sim (0.01 - 0.1)R_{\text{SNR}} \simeq 0.1 - 1$  pc ( $R_{\text{SNR}}$  is gained in Section 3), and giving  $\epsilon_B \sim 0.1$ ,  $L_{\text{sd}} \sim 1.7 \times 10^{34}$  erg s $^{-1}$ , and  $t \sim 3.6$  kyr, one would get  $B_n \sim 1 - 100 \mu\text{G}$ . In this case, a very low  $\text{RM}_{\text{MWN}} \simeq 0.81 \text{ rad m}^{-2} \frac{\text{DM}_{\text{MWN}} B_n}{\text{pc cm}^{-3} \mu\text{G}} \sim 0.01 - 0.3 \text{ rad m}^{-2}$  is acquired through Equation (3). Although some parameters are uncertain, the  $\text{RM}_{\text{MWN}}$  should be low if they fall into reasonable ranges.

(3) Akin to  $\text{DM}_{\text{SNR}}$  estimate,  $\text{RM}_{\text{SNR}}$  in different surrounding environments also has different evolutions.

*ISM Scenario.* In the snowplow phase, the SNR velocity is (Yang & Zhang 2017)

$$v_{\text{SP}} = 690 \text{ km s}^{-1} t_3^{-5/7} E_{51}^{0.445} n_2^{-0.813}. \quad (12)$$

So that the magnetic field generated in the shocked ISM is estimated by (Piro & Gaensler 2018)

$$B_{\text{ISM}} \approx (16\pi\epsilon_B n)^{1/2} v_{\text{SP}} \\ \approx 2.02 \times 10^3 \mu\text{G} \epsilon_{-1}^{1/2} t_3^{-5/7} E_{51}^{0.445} n_2^{-0.313} \quad (13)$$

where  $\epsilon = 10^{-1}\epsilon_{-1}$  is the ratio of the magnetic energy to the shock energy. Hence, the  $\text{RM}_{\text{SNR}}$  in the snowplow phase ( $t > t_{\text{SP}}$ ) deduced from Equations (4) and (13) can be written down as, along with the  $\text{RM}_{\text{SNR}}$  in the Sedov-Taylor phase ( $t < t_{\text{SP}}$ ) (Piro & Gaensler 2018),

$$\text{RM}_{\text{SNR}} \simeq \begin{cases} 1.28 \times 10^5 \text{ rad m}^{-2} \epsilon_{-1}^{1/2} t_3^{-1/5} E_{51}^{2/5} n_2^{11/10}, & t < t_{\text{SP}} \\ 4.94 \times 10^4 \text{ rad m}^{-2} \epsilon_{-1}^{1/2} t_4^{-3/7} E_{51}^{0.67} n_2^{0.424}, & t > t_{\text{SP}} \end{cases} \quad (14)$$

Combining with the result between the energy of the SN explosion  $E$  and the number density  $n$  of ambient ISM in the top panel of Figure 1, one can derive  $\text{RM}_{\text{SNR}}$  as a power-law function of the explosion energy with an index 1.5, as displayed in the left panel of Figure 3. It is also shown that  $\text{RM}_{\text{SNR}}$  can increase up to  $10^3 \text{ rad m}^{-2}$  when  $E$  approaches to  $10^{52}$  erg.

*Wind Scenario.* The  $\text{RM}_{\text{SNR}}$  in wind environment is calculated by (Piro & Gaensler 2018)

$$\text{RM}_{\text{SNR}} \simeq \begin{cases} 0.002 \text{ rad m}^{-2} x_{0.1} R_{*,2} B_{*,0} \mu_e^{-1} E_{51}^{-1} M_1 t_3^{-2}, & t < t_{\text{ch}} \\ 0.0017 \text{ rad m}^{-2} x_{0.1} R_{*,2} B_{*,0} \mu_e^{-1} E_{51}^{-2/3} K_{13}^{5/3} t_4^{-4/3}, & t > t_{\text{ch}} \end{cases} \quad (15)$$

where  $x \equiv v_{\text{rot}}/v_w$  ( $v_{\text{rot}}$  and  $v_w$  are the rotation velocity and wind velocity),  $R_* = 100R_{\odot} R_{*,2}$  and  $B_* = 10^0 B_{*,0}$  G are the progenitor's radius and magnetic field, respectively. Fixing  $x = 0.1$ ,  $R_* = 100R_{\odot}$ ,  $\mu_e = 1$ , and  $B_* = 1$  G (even if they should be variable for different types of progenitors), and using the relation between the energy of the SN explosion  $E$  and the parameter  $K$  in the top panel of Figure 2 for different progenitors ( $M = 2M_{\odot}$  and  $M = 10M_{\odot}$ ), one gains a low  $\text{RM}_{\text{SNR}} < 2 \text{ rad m}^{-2}$  when the explosion energy  $E < 10^{52}$  erg, as exhibited in the right panel of Figure 3.

Note that the foreground  $\text{RM} = +223 \pm 2 \text{ rad m}^{-2}$  for SNR G57.2+0.8 (Kothes et al. 2018) and a highly polarised radio burst with  $\text{RM}_{\text{obs}} = +112.3 \text{ rad m}^{-2}$  for SGR 1935+2154 (Zhang et al. 2020a). If SGR 1935+2154 and SNR G57.2+0.8 is actually related to each other and the foreground  $\text{RM}$  has no contribution from the local environment of the SNR, it could indicate that the  $\text{RM}_{\text{SNR}} \sim -110 \text{ rad m}^{-2}$ , suggesting a possible explosion energy  $E \sim 2 \times 10^{51}$  erg in the ISM scenario for the SNR from the left panel of Figure 3.

## 5. CONCLUSIONS

In this paper, we have utilized DM contributed by the foreground ISM of our Galaxy and the local environments including the magnetar wind nebula and SNR to estimate the distance of SGR 1935+2154 potentially hosted in SNR G57.2+0.8, assuming the SGR and SNR are realistically related and combining with the observational constraints. Besides, the  $\text{RM}$  estimate and results have been also discussed. Some interesting results are as follows:

- In the constant ISM scenario for the SNR, the energy of the SN explosion  $E$  has a power-law function as the ambient medium density  $n$  with an index 1.0. Moreover, the distance, SNR radius, and DM contributed by the SNR narrowly distribute  $D \simeq 9.06 - 9.11$  kpc,  $R_{\text{SNR}} \simeq 14.5 - 14.6$  pc, and  $\text{DM}_{\text{SNR}} \simeq 0 - 5 \text{ pc cm}^{-3}$  in a typical region of the explosion energy, respectively.
- In the wind scenario for the SNR, the distance, SNR radius and  $\text{DM}_{\text{SNR}}$  also spread over similar ranges of those in the ISM scenario for different

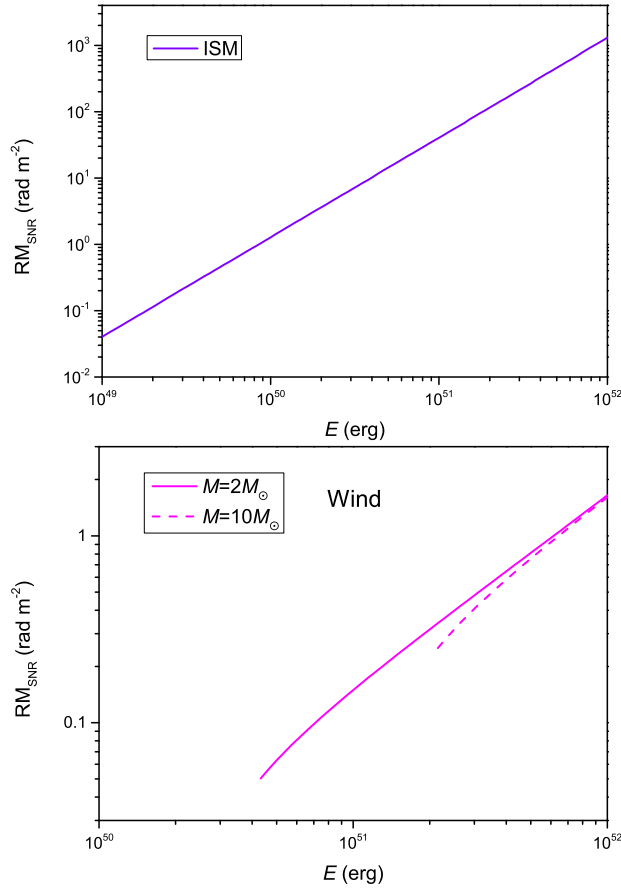


**Figure 3.** The  $RM_{SNR}$  vs. the energy of explosion  $E$  in ISM (left panel) and wind (right panel) environments.

mass of the SN ejecta. But the acceptable explosion energy is more confined.

- For the RM estimate, the polarization observations from the radio burst of the SGR and the intensity maps of the SNR might signify that the RM contribution by the local environment of the SNR is about  $-110 \text{ rad m}^{-2}$  corresponding to the explosion energy  $\sim 2 \times 10^{51} \text{ erg}$  in the ISM scenario for the SNR.

On the whole, our results relevant to DM are basically in agreement with the previous studies but seem to be tighter.

#### ACKNOWLEDGMENTS

We would like to thank Wei-Li Lin for her helpful discussions. This work was supported by the National Key Research and Development Program of China (grant No. 2017YFA0402600) and the National Natural Science Foundation of China (grant No. 11833003). C.M.D. is partially supported by the Fundamental Research Funds for the Central Universities (NO. WK2030000019).

#### REFERENCES

- Bochenek, C. D., Ravi, V., Belov, K. V., et al. 2020, arXiv e-prints, arXiv:2005.10828. <https://arxiv.org/abs/2005.10828>
- Cao, X.-F., Yu, Y.-W., & Dai, Z.-G. 2017, ApJL, 839, L20, doi: 10.3847/2041-8213/aa6af2
- Cordes, J. M., & Lazio, T. J. W. 2002, arXiv e-prints, astro. <https://arxiv.org/abs/astro-ph/0207156>
- Draine, B. T. 2011, Physics of the Interstellar and Intergalactic Medium (Princeton, NJ: Princeton Univ. Press)
- Gaensler, B. M. 2014, GRB Coordinates Network, 16533, 1
- Han, J. L., & Qiao, G. J. 1994, A&A, 288, 759
- Israel, G. L., Esposito, P., Rea, N., et al. 2016, MNRAS, 457, 3448, doi: 10.1093/mnras/stw008
- Jansson, R., Farrar, G. R., Waelkens, A. H., & Enßlin, T. A. 2009, JCAP, 2009, 021, doi: 10.1088/1475-7516/2009/07/021
- Kothes, R., Sun, X., Gaensler, B., & Reich, W. 2018, ApJ, 852, 54, doi: 10.3847/1538-4357/aa9e89
- Kozlova, A. V., Israel, G. L., Svinkin, D. S., et al. 2016, MNRAS, 460, 2008, doi: 10.1093/mnras/stw1109
- Li, C. K., Lin, L., Xiong, S. L., et al. 2020, arXiv e-prints, arXiv:2005.11071. <https://arxiv.org/abs/2005.11071>
- Lin, W.-L., & Dai, Z.-G. 2016, Research in Astronomy and Astrophysics, 16, 38, doi: 10.1088/1674-4527/16/3/038
- Lyman, J. D., Bersier, D., James, P. A., et al. 2016, MNRAS, 457, 328, doi: 10.1093/mnras/stv2983
- Mereghetti, S., Savchenko, V., Ferrigno, C., et al. 2020, arXiv e-prints, arXiv:2005.06335. <https://arxiv.org/abs/2005.06335>
- Metzger, B. D., Berger, E., & Margalit, B. 2017, ApJ, 841, 14, doi: 10.3847/1538-4357/aa633d
- Pavlović, M. Z., Urošević, D., Vukotić, B., Arbutina, B., & Göker, Ü. D. 2013, ApJS, 204, 4, doi: 10.1088/0067-0049/204/1/4
- Pejcha, O., & Prieto, J. L. 2015, ApJ, 806, 225, doi: 10.1088/0004-637X/806/2/225

- Piro, A. L., & Gaensler, B. M. 2018, *ApJ*, 861, 150, doi: [10.3847/1538-4357/aac9bc](https://doi.org/10.3847/1538-4357/aac9bc)
- Prouza, M., & Šmída, R. 2003, *A&A*, 410, 1, doi: [10.1051/0004-6361:20031281](https://doi.org/10.1051/0004-6361:20031281)
- Pshirkov, M. S., Tinyakov, P. G., Kronberg, P. P., & Newton-McGee, K. J. 2011, *ApJ*, 738, 192, doi: [10.1088/0004-637X/738/2/192](https://doi.org/10.1088/0004-637X/738/2/192)
- Ranasinghe, S., Leahy, D. A., & Tian, W. 2018, *Open Physics Journal*, 4, 1, doi: [10.2174/1874843001804010001](https://doi.org/10.2174/1874843001804010001)
- Ridnaia, A., Svinkin, D., Frederiks, D., et al. 2020, arXiv e-prints, arXiv:2005.11178. <https://arxiv.org/abs/2005.11178>
- Sedov, L. I. 1959, *Similarity and Dimensional Methods in Mechanics* (New York: Academic Press)
- Simard-Normandin, M., & Kronberg, P. P. 1980, *ApJ*, 242, 74, doi: [10.1086/158445](https://doi.org/10.1086/158445)
- Stanev, T. 1997, *ApJ*, 479, 290, doi: [10.1086/303866](https://doi.org/10.1086/303866)
- Sun, X.-H., & Reich, W. 2010, *Research in Astronomy and Astrophysics*, 10, 1287, doi: [10.1088/1674-4527/10/12/009](https://doi.org/10.1088/1674-4527/10/12/009)
- Sun, X. H., Reich, W., Waelkens, A., & Enßlin, T. A. 2008, *A&A*, 477, 573, doi: [10.1051/0004-6361:20078671](https://doi.org/10.1051/0004-6361:20078671)
- Surnis, M. P., Joshi, B. C., Maan, Y., et al. 2016, *ApJ*, 826, 184, doi: [10.3847/0004-637X/826/2/184](https://doi.org/10.3847/0004-637X/826/2/184)
- Tavani, M., Casentini, C., Ursi, A., et al. 2020, arXiv e-prints, arXiv:2005.12164. <https://arxiv.org/abs/2005.12164>
- Taylor, G. 1950, *Proceedings of the Royal Society of London Series A*, 201, 159, doi: [10.1098/rspa.1950.0049](https://doi.org/10.1098/rspa.1950.0049)
- The CHIME/FRB Collaboration, :, Andersen, B. C., et al. 2020, arXiv e-prints, arXiv:2005.10324. <https://arxiv.org/abs/2005.10324>
- Tinyakov, P. G., & Tkachev, I. I. 2002, *Astroparticle Physics*, 18, 165, doi: [10.1016/S0927-6505\(02\)00109-3](https://doi.org/10.1016/S0927-6505(02)00109-3)
- Yang, Y.-P., & Zhang, B. 2017, *ApJ*, 847, 22, doi: [10.3847/1538-4357/aa8721](https://doi.org/10.3847/1538-4357/aa8721)
- Yao, J. M., Manchester, R. N., & Wang, N. 2017, *ApJ*, 835, 29, doi: [10.3847/1538-4357/835/1/29](https://doi.org/10.3847/1538-4357/835/1/29)
- Yu, Y.-W. 2014, *ApJ*, 796, 93, doi: [10.1088/0004-637X/796/2/93](https://doi.org/10.1088/0004-637X/796/2/93)
- Zhang, C. F., Jiang, J. C., Men, Y. P., et al. 2020a, *The Astronomer's Telegram*, 13699, 1
- Zhang, S. N., Tuo, Y. L., Xiong, S. L., et al. 2020b, *The Astronomer's Telegram*, 13687, 1
- Zhang, S. N., Zhang, B., & Lu, W. B. 2020c, *The Astronomer's Telegram*, 13692, 1
- Zhang, S. N., Xiong, S. L., Li, C. K., et al. 2020d, *The Astronomer's Telegram*, 13696, 1
- Zhou, P., Zhou, X., Chen, Y., et al. 2020, arXiv e-prints, arXiv:2005.03517. <https://arxiv.org/abs/2005.03517>